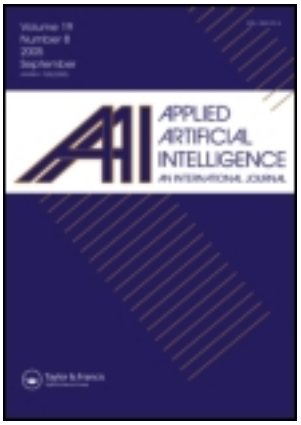

Applied Artificial Intelligence: An International Journal

Publication details, including instructions for authors and subscription information:
http://www.tandfonline.com/loi/uaai20

RANGE-LIMITED UAV TRAJECTORY USING TERRAIN MASKING UNDER RADAR DETECTION RISK

Michael Pelosi [a], Carlo Kopp [b] & Michael Brown [c]

[a] Nova Southeastern University, Fort Lauderdale, Florida

[b] Monash University, Victoria, Australia

[c] Valhalla Data Systems, Germantown, Maryland

Version of record first published: 14 Sep 2012.

To cite this article: Michael Pelosi, Carlo Kopp & Michael Brown (2012): RANGE-LIMITED UAV TRAJECTORY USING TERRAIN MASKING UNDER RADAR DETECTION RISK, Applied Artificial Intelligence: An International Journal, 26:8, 743-759

To link to this article: http://dx.doi.org/10.1080/08839514.2012.713308

Applied Artificial Intelligence, 26:743–759, 2012

ISSN: 0883-9514 print/1087-6545 online
DOI: 10.1080/08839514.2012.713308

Taylor & Francis
Taylor & Francis Group

RANGE-LIMITED UAV TRAJECTORY USING TERRAIN MASKING UNDER RADAR DETECTION RISK

Michael Pelosi[1], Carlo Kopp[2], and Michael Brown[3]
[1]*Nova Southeastern University, Fort Lauderdale, Florida*
[2]*Monash University, Victoria, Australia*
[3]*Valhalla Data Systems, Germantown, Maryland*

□ *Military manned and unmanned aerial vehicles (UAVs) may perform missions in contested airspace, where survival of the vehicle requires avoidance of hostile radar coverage. This research sought to determine optimum flight-path routes that make maximum utilization of UAV terrain-masking opportunities and flight range capability to avoid radar detection. The problem was formulated as one of constrained optimization in three dimensions; advantageous solutions were identified using Algorithm A*. Topographical features were exploited by the algorithm to avoid radar detection. The model included provisions for preferred altitude ranges, adjustable aircraft climb- and descent- rate envelopes, movement costs based on fractional detection probability, radar horizon masking, and simulated radar cross-section lookup tables.*

INTRODUCTION

Military aircraft often perform missions in contested airspace, where air vehicle survival depends on the avoidance of line-of-sight weapons and supporting sensors. Because terrain and other solid objects block optical and microwave band electromagnetic waves, an object cannot be detected if it is flying behind terrain in relation to the position of the sensor. Moreover, smaller air vehicles can exploit terrain features for masking, which larger aircraft would not be able to maneuver around or within.

Historically, the military exploitation of terrain-masking techniques first emerged during the 1940s, with the advent of optically aimed and microwave radar directed air defense weapons, all of which require geometrical line of sight to a target.

Address correspondence to Michael Pelosi, 18459 Pines Blvd. #422, Pembroke Pines, FL 33029, USA. E-mail: mpelosi@maui.net

The first technology specifically developed to facilitate such penetration techniques was the terrain avoidance radar, soon followed by the terrain following radar (USAF 1969, 1973). The aircrew would plan a sortie around the known locations of air defenses and known terrain and would exploit the radar to maintain safe terrain clearances during flight. Effectiveness was constrained by the time invested in understanding the terrain features and threat placement, and the ability of the aircrew to employ the radar effectively. This technology remains in use on a wide range of manned aircraft, both fixed wing and rotary wing, intended to penetrate contested airspace.

The advent of high-performance-embedded computing hardware, high-fidelity geographical information systems (GIS), and related technologies for exploiting spatial information, has presented further opportunities for the use of terrain masking. A number of systems that exploit terrain elevation databases have been developed to aid rotary-wing aircrews in penetrating contested airspace (Kopp 2009a).

Such technologies are especially useful when employed with Uninhabited Aerial Vehicles (UAV), which can employ highly automated digital autopilot systems (Hasircioglu, Topcuoglu, and Ermis 2008). Such designs permit many UAVs to execute missions autonomously and thus independently of direct operator control.

PREVIOUS RESEARCH

Recent research, which is prolific in this area, aims to find more efficient and effective route-planning methods for UAVs (Ruz et al. 2007). A range of metrics can be employed for assessing both efficiency and effectiveness of a route-planning methodology. In the case of avoiding radar detection, there are several critical parameters that can be used in constructing metrics for comparison purposes. Probability of detection along a specific leg of the path, the length of this detection distance, and the duration of a respective exposure are examples of critical parameters. Reducing the values of any of these parameters will serve to reduce the exposure to overall radar detection risk.

Routes with greater efficiency over human planning and various established methods have been demonstrated using mixed-integer linear programming (MILP; Ruz et al. 2006), the A* algorithm (Quigley et al. 2005), evolutionary algorithms (de la Cruzet al. 2008; Nikolos, Tsourveloudis, and Valavanis 2001), and several other techniques (such as in Karim and Heinze 2005). Vincent and Rubin (2004) proffered a framework and analysis for cooperative search using UAV swarms. Implementation and flight test results of mixed-integer linear-programming-based UAV guidance is the subject of the Schouwenaars et al. (2005) paper.

Kamrani and Ayani (2007) suggested a simulation-aided path-planning method for UAVs. Their method uses sequential Monte Carlo simulation. UAVs' path planning for searches and other goals has also been demonstrated using genetic algorithms (Russell and Lamont 2005), dynamic programming (Flint, Fernandez, and Kelton, in press), Bayesian updating, reactive tabu search (Ryan et al. 1998), and evolving cooperative control (Barlow, Oh, and Smith 2008), among others.

Ruz et al. (2006, 2007) and Pajares et al. (2008) developed methods that were used as a foundation for this study. De la Cruz et al. (2008) explicitly built on the work of Pajares et al. (2008) and developed an evolutionary path planner for UAVs in realistic environments. Hasircioglu, Topcuoglu, and Ermis (2008) further developed the notion of 3D path planning for the navigation of unmanned vehicles using evolutionary algorithms.

A radar model for the instantaneous probability of radar detection of an aircraft has been derived from Zabarankin, Uryasev, and Murphey (2006), and was used for the purposes of this research to estimate probabilities of radar detections during route planning.

METHODOLOGY

A software simulation environment was created for the purpose of investigating the methods of the completed research. The design of the simulation environment incorporated the following major divisions: the model inputs, a terrain surface model, a radar detection model, a flight-path model, and Algorithm A* implementation.

Figure 1 shows a graphic depiction of the breakdown of the implemented methodology. The methodology establishes a 3D flight-space and map environment of gridded cells, places radar sites (with various range and detection capabilities) on the surface of the terrain map at various locations, and attempts to find a radar detection avoiding path from a start location to a goal location subject to the flight limitations of the UAV. This path is computed using Algorithm A*.

These divisions are further described as follows.

The Model Inputs

The simulation model inputs consisted of the following:

1. A terrain map consisting of grid-squares encoded with vertex (grid-square corner) elevations above sea level
2. Single or multiple radar types (along with radar model coefficient values for c_1 and c_2) and locations (X, Y, Z coordinates)

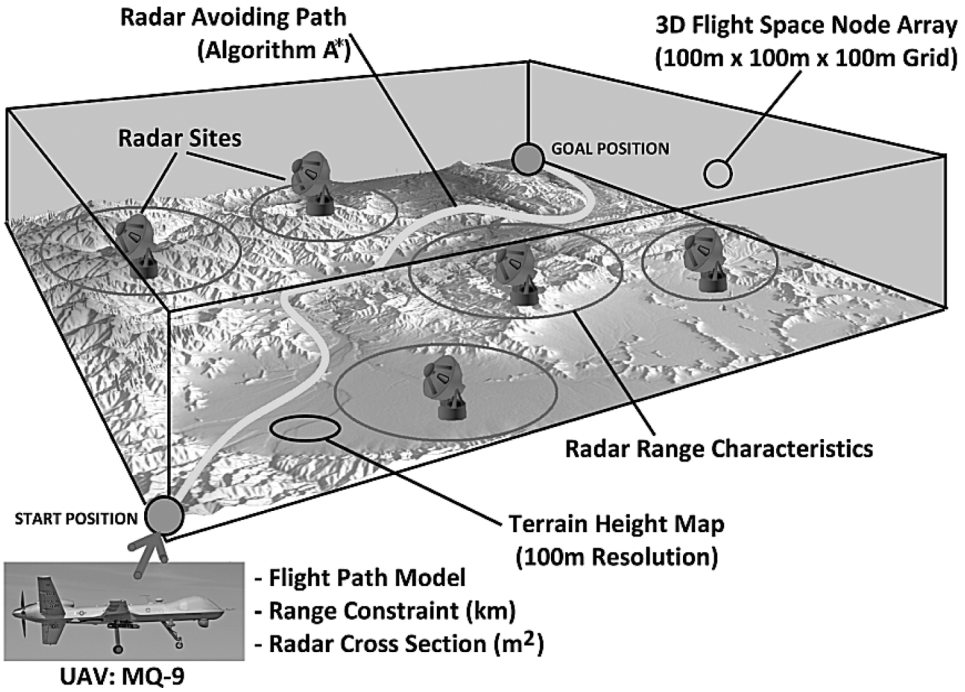

FIGURE 1 Graphical depiction of a breakdown of the research method.

3. UAV mission range constraint in km
4. UAV radar cross section (RCS) in m^2
5. UAV start and goal cells
6. Threshold radar detection probability, $p_{\min}$

These inputs were employed to constrain the simulation. The terrain map provides information defining and thus constraining the geometrical properties of the terrain that is to be exploited for masking. The radar-type parameters constrain detection range performance and thus also probability of detection. The RCS parameters are characteristic of the air vehicle, and vary with radar wavelength and viewing aspect relative to the air vehicle.

Terrain Surface Model

The terrain surface model consists of grid squares divided at the 100-meter intervals matching the flight-path model. Sample terrain-elevation data were matched to each grid-square vertex. UAV flight-path

altitudes were limited to values above this terrain surface elevation. Terrain elevation values were also used to test whether radar-blocking terrain existed in the lineof sight (LOS) between the radar and the UAV. Specifically, the straight line between the radar and UAV was tested. If any point along the line was found to be below the terrain surface, a blockage existed.

Radar Detection Model

The instantaneous probability of radar detection of an aircraft by Zabarankin, Uryasev, and Murphey (2006) is shown in Equation (1):

$$P = \frac{1}{1 + \left(\frac{c_2 R^4}{\sigma}\right)^{c_1}}. \tag{1}$$

This simple model of radar detection was used for the completed research, granting that other models may yield much better results. Lumped coefficient values of c_1 and c_2 were obtained for several radars, and RCS (σ) values were obtained for several sample UAVs. The Euclidean distance between a radar and UAV was used as a range (R) value, and providing that there were no solid objects extant between the radar and the UAV, a detection probability (P) was calculated. If the probability of detection was below the specified threshold value, $p_{\min}$, the probability of detection was set to zero. The range at $p_{\min}$ was considered the maximum radar detection range, $R_{\max}$.

For route determination, cells at range greater than or equal to $R_{\max}$ had their radar signature set to zero. A ray-casting technique to be described was used to determine cell radar visibility out to range $R_{\max}$ for individual cells. If solid terrain existed in the LOS between the radar and any cell location out to range $R_{\max}$, the cell visibility (detection) was set to zero. Otherwise, the cell retained a detection value of unity. Cells with nonzero radar detection values were considered radar detectable in objective function evaluations. Figure 2 shows an example of radar terrain masking. Objects below the mask angle produced by the screening crest were not detectable.

Flight-Path Model

The radar detection avoidance problem used 3D path optimization in Euclidean space. UAV movement paths minimizing detection were calculated through a series of cells, between the start cell and the goal cell. In the simulation environment, Euclidean space was divided into a series of

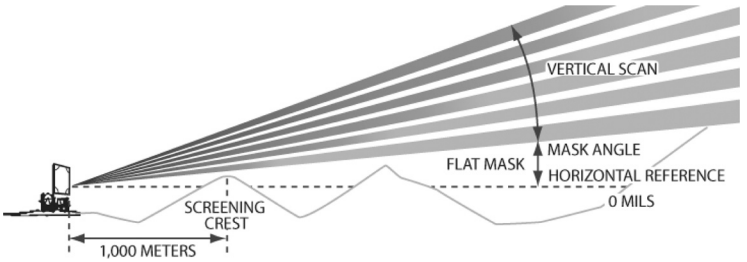

FIGURE 2 Example of solid terrain screening (masking) radar line of sight.

cells (nodes) 100 m wide in the X dimension, 100 m long in the Z dimension, and of variable height in the Y dimension to adjust for aircraft maximum climb rates.

Algorithm A* Implementation

Algorithm A* implementation was included, using the objective function and weighting constant previously mentioned. The computed paths represented a shared emphasis of short distance and minimized probability of radar detection through the variance of a weighing constant. Other route-finding methods were also considered.

Objective Function

The inherent goal of the route-planning approach was to identify a path from a start cell s to a goal cell g such that the following objective function in Equation (2) was minimized:

$$f(path[s,g]) = \alpha.d(path[s,g]) + (1-\alpha)r(path[s,g]), \tag{2}$$

where:

$path[s,g]$ = A sequence of adjacent cells that defines a path from start cell s to goal cell g.
$d(path[s,g])$ = The distance traveled through the cells in $path[s,g]$.
$r(path[s,g])$ = The radar detectable weighted distance through cells in $path[s,g]$.
α = A weighting constant ranging from 0 to 1;
with $\alpha = 1$ the objective is to minimize the total path distance,
and with $\alpha = 0$ the objective is to minimize the radar detectable weighted distance traveled.

Evaluation Strategy

An evaluation strategy serves to offer the criteria by which the qualities of the research method can be judged versus other methods. For comparison, criteria can be either qualitative or quantitative. If quantitative, numeric measures are calculated and then compared from before and after the research method application. In order to measure the efficacy of the route-planning algorithm, radar detection risks of computed least cost distance paths (weighting constant $\alpha = 1$) were compared to paths computed using the algorithm set for maximum radar detection avoidance within the UAV flight-range constraint (in this case the value of the weighting constant α was determined through the process shown in Figure 3). The relative reduction of flight path total radar tracking distance between least-distance cost paths and that computed using maximum radar avoidance at the range limit were compared. A chart of the effects of changing the value of α is shown in Figure 4.

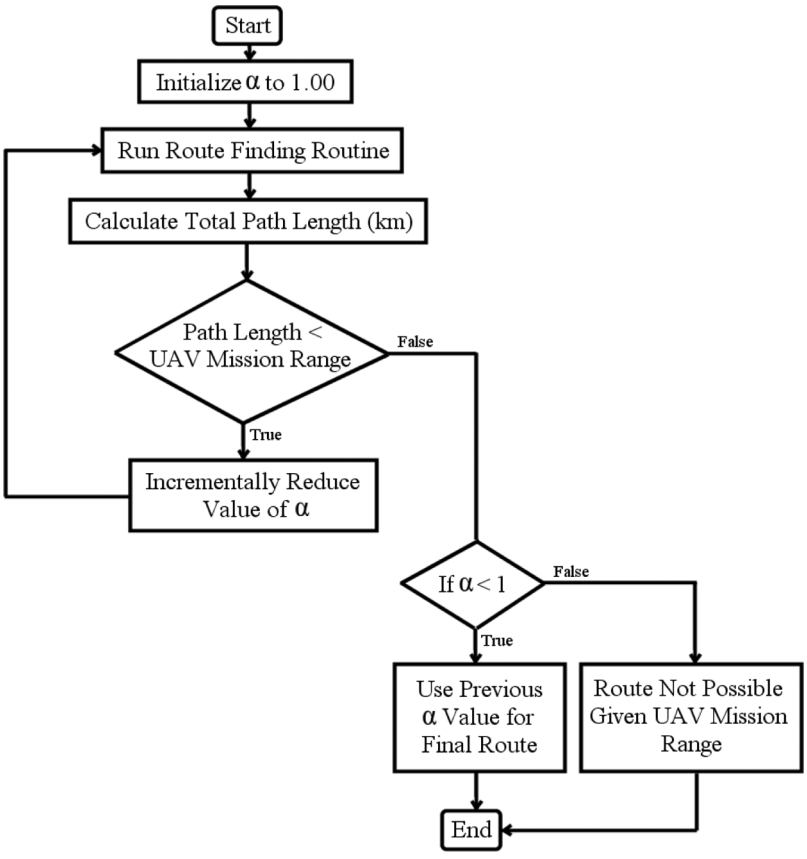

FIGURE 3 Process for finding value of weighting constant α that results in a maximum radar detection avoidance path at the limit of UAV flight range.

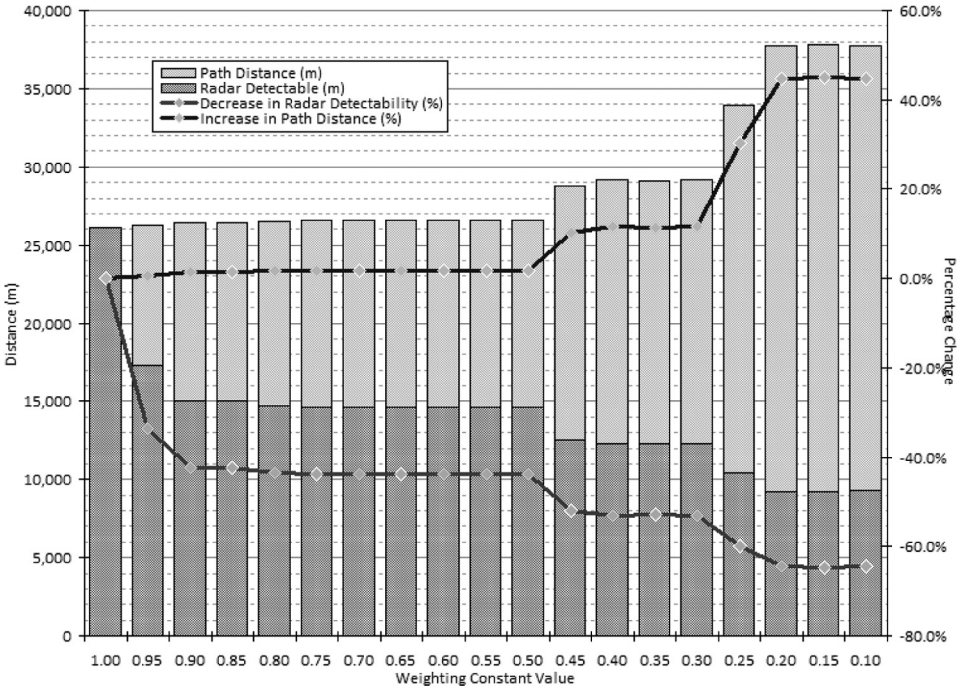

FIGURE 4 As the weighting constant α is decreased, radar detectability decreases (shown in dark shading) and total path length tends to increase (shown in light shading).

As a benchmark evaluation standard, if the total radar tracking distance is reduced below a specific threshold value, a UAV would be unable to be shot down while traveling its assigned path. This is because a UAV must be radar tracked for a specific distance before it can be acquired as a potential target by enemy air defense, and then consecutively radar tracked while any launched missiles are guided to a physical impact (Kabamba, Meerkov, and Zeitz 2006). This is because most air defense missiles employ command guidance via a radio uplink channel, which requires continuous and frequent updates to correct the missile trajectory. Anti-aircraft artillery (AAA) and directed energy weapons (DEW) such as lasers share this property. The only exceptions are some short-range air defense missiles that employ terminal homing seekers, such as infrared scanning seekers. The latter are capable of fully autonomous self-guidance once launched (Kopp 2008, 2009c; Andrew 2009).

Resources

Open source elevation data from the Shuttle Radar Topography Mission (SRTM90) were used to construct three-dimensional terrain models of areas of interest. SRTM90 data are available in geographically

referenced terrain-elevation cells nominally spaced at 90-meter intervals. These data are easily interpolated into consistent 100-meter per-side grid squares.

Altitude Movement Cost Penalty

In certain mission situations it may be desirable that, in addition to avoiding radar detection, a UAV or aircraft fly at a relatively low or high altitude. This may be a secondary or tertiary goal in addition to avoiding radar detection. Examples of when a mission overall low-flight altitude may be desirable may be to avoid possible visual detections by nonaligned forces, to decrease the probability of detection by unknown radars, and to avoid aircraft known or possibly present at higher altitudes. Examples of the potential benefits of flying where possible at high altitudes include avoiding small arms fire from ground personnel, avoiding air defense point defense weapons that may be present in the area (such as antiaircraft artillery or MANPADS), avoiding antiaircraft minefields, conserving fuel by maintaining a more steady and engine-power-efficient altitude, and reducing the likelihood of collision with undocumented surface objects, elevated foliage canopies or terrain. By introducing an altitude movement cost penalty into the objective function, low- or high-altitude flight can be encouraged that is weighted in the same proportion as movement distance is weighted in relation to the weighting constant α.

Fractional Probability and Multiple Radar Detection Based Movement Costs

Overall cell probabilities of detection are calculated for multiple radars, each of which has an individual cell probability of detection greater than or equal to $p_{\min}$. This calculation relies on the fact that each of up to n radars can individually detect and track a UAV probabilistically. At each observation, time detection and tracking by any radar are independent from those of any other radar. Let P_{t1} be the probability of the event that the UAV is tracked by a first radar. Let P_{t2} be the probability of the event that the UAV is tracked by a second radar. Let P_t be the probability of the union of these two events. Under the condition of tracking independence,

$$\begin{aligned} P_t &= P_{t_1} + P_{t_2} - P_{t_2}P_{t_2}, \\ P_t &= 1 - (1 - P_{t_1})(1 - P_{t_2}) \end{aligned}. \tag{3}$$

The output P_t from Equation (3) represents the probability that the UAV is tracked by an overall integrated air defense network that includes

all radars on the map. For n such radars sharing tracking information within the network, the network could be considered to track the UAV when any of the n radars is tracking it. Equation (3) above can be extended to the event that any of n radars is tracking the UAV as in Equation (4),

$$P_t = 1 - (1 - P_{t_1})\left(1 - P_{t_2}\right) \ldots (1 - P_{t_n}). \tag{4}$$

Equation (4) computes a cell overall cumulative detection probability that includes consideration of multiple radars. P_t is greater than or equal to the maximum probability of track for any of the n radars individually, $P_t \geq \max\{P_{t1}, P_{t2}, \ldots, P_{tn}\}$, indicating the synergistic nature of an integrated air defense network comprising multiple radars working cooperatively.

Using the approach described above, final mission movement paths computed by the simulation environment report a radar detectable equivalent distance. This is simply a distance value in meters that has been normalized for changing probabilities of detection. Distances are weighted for the cumulative probability of detection at each increment.

Radar Horizon Masking

The curvature of Earth can mask radar detection at sufficiently long ranges, similarly to the masking by elevated terrain features already discussed. A simplified illustration of this effect is shown in Figure 5.

Refractive effects arising in the atmosphere as a result of altitude dependent gradients and local variations in density and humidity can often produce significant variations in the distance to the horizon, which are applicable to both microwave radar and optical sensors. Considerable research has been performed on the subject of refraction, but it is fragmented across a range of research communities. Effects that can significantly alter horizon ranges compared to the geometrical horizon include subrefraction, superrefraction and inversion. The most commonly

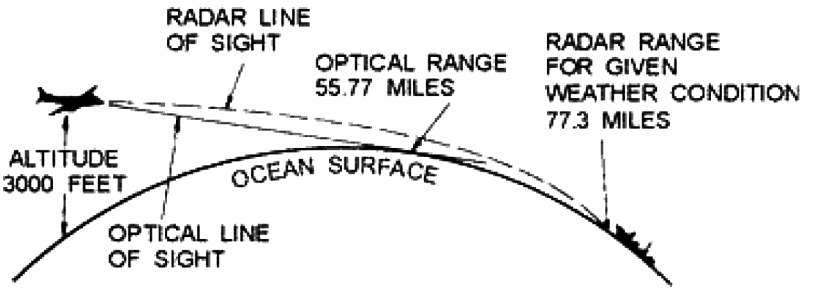

FIGURE 5 Difference between optical and radar horizon lines of sight.

employed refractive correction models are based on the spherical "effective Earth radius" approximation, or variants of the exponential atmosphere model (Schelleng, Burrows, and Ferrell 1933; Kopp and Wallace 2004).

At shorter ranges and under temperate climatic conditions, the Schelling, Burrows, and Ferrell (1933) (SBF) model performs adequately, and remains widely used in simulation tools. The important caveat in simulation applications is that the model may become quite inaccurate in environments with atypical atmospheric density and humidity gradients, such as deserts and dense jungles, where subrefraction and superrefraction may arise. Under such conditions, an adjusted "effective Earth radius" value must be employed (Kopp 2010).

In practical terms, common atmospheric refractive conditions will slightly increase detection ranges, in comparison with a vacuum, and this must be accounted for when modeling terrain masking performance.

Elevating a sensor such as radar, for example on a mast, will directly increase its useful detection range against low-altitude aircraft (see Figure 6). This is because of an increased distance to the radar horizon and elevation of the antenna phase center above obstructing terrain features. Given a strongly refracting environment and weak fading effects, antenna elevation can yield strong improvements in long-range radar detection range performance. The simulation environment allows the option of placing radars at various elevations above surrounding terrain.

RCS Modeling: Isotropic, Ellipsoidal, and Physical Optics Based Method Options

Examples of the field measurement of actual radar cross section (RCS) values as a function of aircraft aspect and elevation angles, measured in decibels relative to a square meter (dBSM), make clear that the RCS

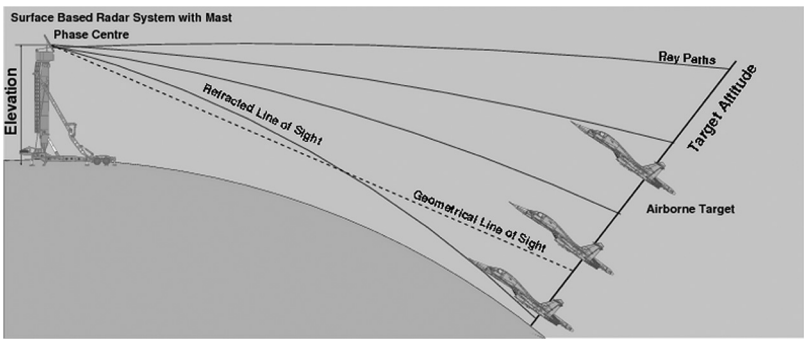

FIGURE 6 Extended radar low-altitude detection range with radar mounted on 24 m above-ground mast.

presented to radar varies widely depending on aircraft aspect presented to the radar, as well as radar operating wavelength. Most research in terrain-masking algorithms thus far has used a single, invariant, isotropic RCS value for all aircraft aspects. This naïve approach can yield large errors, as aspect and wavelength variations in RCS performance of typical air vehicles may span several orders of magnitude.

In the literature, an example of a nonisotropic RCS model used for an aircraft is that of an ellipsoid (Kabamba, Meerkov, and Zeitz 2006). Although the ellipsoid model does not represent the RCS of a specific aircraft, it captures three important characteristics: a relatively small nose- or tail-aspect RCS, a larger beam (side)-aspect RCS, and a relatively large RCS when the aircraft is viewed from above or below.

In order to improve the accuracy of RCS modeling, the ellipsoid RCS model described by Kabamba has been implemented as an optional RCS model in the software. The RCS value output from this ellipsoid model based on aircraft aspect and bank angles varies greatly. Sample values range from -20 dBSM ($\times 0.01$) nose- or tail-on, to 0 dBSM ($\times 1$) from either side of the aircraft, to $+10$ dBSM ($\times 10$) from top or bottom. This corresponds to a range variation of three magnitudes and improves greatly on the isotropic model.

We employed a model for the MQ-9 Reaper UAV for this simulation (see Figure 7). The MQ-9 is a variable-altitude, long-endurance, remotely piloted aircraft system, whose primary mission is armed intelligence, surveillance and reconnaissance (ISR). This vehicle employed multiple sensors to provide data to intelligence specialists at all military and civilian echelon levels. We employed the physical optics facet simulator (POFACETS), previously developed at the Naval Postgraduate School, which uses the Physical Optics method to predict the RCS of complex targets,

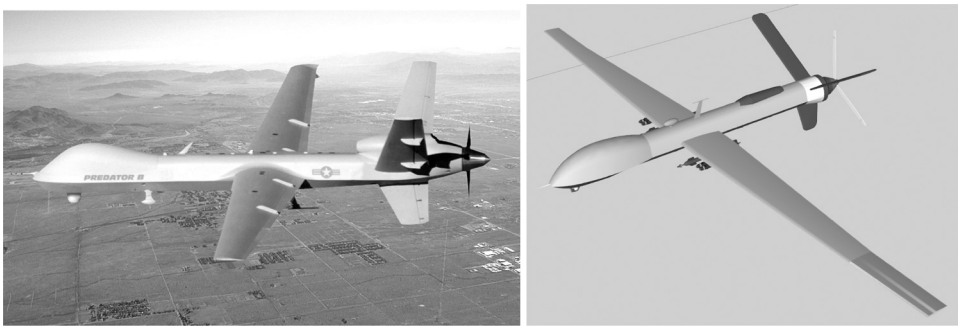

FIGURE 7 Left: the MQ-9 Reaper UAV. Right: 3D model used for RCS simulation (armed with 4× AGM-114 Hellfire air-to-ground missiles and 2×500 lb GBU-12 Paveway II laser-guided bombs).

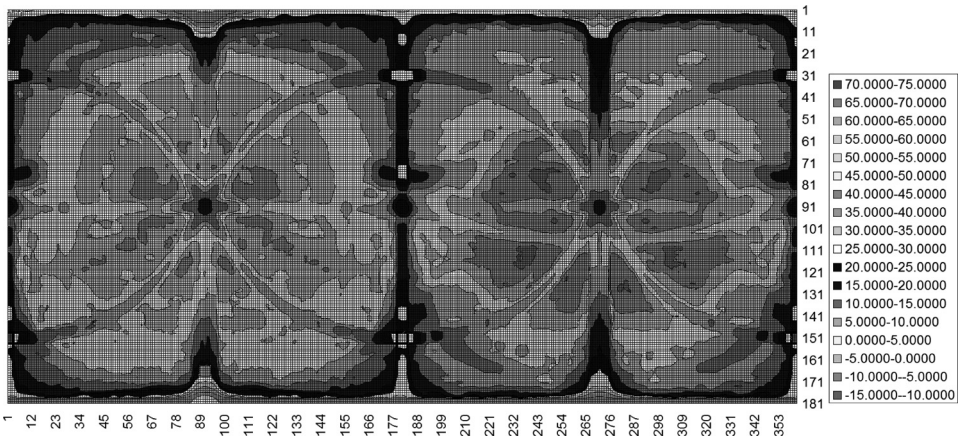

FIGURE 8 Simulated MQ-9 (2.7 GHz) RCS aspect and elevation angle lookup table values (dBSM).

represented by arrays of triangular facets. Code from this program was ported to a custom utility, which also incorporated effects that were a result of geometric object self-shadowing. The RCS of the MQ-9 Reaper UAV at 0–360 degree aspect and 0–180 degree elevation angles was then estimated at 2.7 GHz (the S-band frequency of the 76N6 radar), as depicted in Figure 8. These 64,800 aircraft-perspective orientation values were smoothed over a 5-degree moving average and incorporated into a lookup table that was accessed by the radar detection model in the simulation environment. Based on the aspect of the UAV relative to a potentially detecting radar, the corresponding RCS signature value was retrieved as needed for use in Equation (1) as σ (RCS m^2).

RESULTS

To produce representative simulation results, the model needed to include a representative air vehicle (MQ-9) and a representative threat system and sensor.

We employed the widely used Russian S-300P surface-to-air missile system as a representative threat. The S-300 PM, PMU, PMU1 and PMU2 (SA-10 Grumble and SA-20 Gargoyle) are produced by NPO Almaz. These systems were developed for the Soviet Air Defense Forces during the Cold War to defend against penetrating aircraft and cruise missiles at all altitudes. Later variants can intercept tactical ballistic missiles. Figure 9 shows an S-300PMU1 5P58SE system high-mobility missile Transporter-Erector-Launcher (TEL) vehicle mounting four sealed launch tubes and the mast-mounted Lianozovo (LEMZ) 5N66/76N6E Clam Shell radar.

FIGURE 9 (a) S-300PM/PMU system 48N6E SAM TEL launch vehicle, (b) and (c) 76N6 Clamshell low-altitude early-detection radar, with 23.8 m and 38.8 m 40V6 M and 40V6MD mounting masts, respectively.

For modeling purposes, the S-band LEMZ 76N6 Clam Shell series radars are especially interesting, as they have been widely exported as part of the S-300PMU (SA-10B) and S-300PMU1 (SA-20A) systems. The 76N6E is a specialized, low-altitude acquisition radar, intended for engagements against low-flying targets, including aircraft and low RCS cruise missiles.

The Russian LEMZ Corporation, manufacturer of the 76N6E, has published specifications indicating a 50% probability of detection of an aircraft with a $0.02\,m^2$ RCS value at 500 m altitude and at a range of 90 km (Kopp 2004).

The 76N6 Clam Shell, mounted on a 38.8-meter phase center NKMZ 40V6MD semimobile mast was modeled in the simulation environment as the benchmark radar model to plot covert paths around and through. The mast is optional equipment for the 76N6E, 30N6E Flap Lid/Tomb Stone, ST-68UM Tin Shield and 96L6E S-300P system radars. Employment of the 40V6MD substantially improves low-altitude detection range capabilities of all of these radar types (Kopp 2009b).

A test was done using a 100 km × 100 km area map centered on latitude 56.68° N and longitude 34.96° E. Two 76N6 radars were diametrically placed (northwest and southeast), resulting in the route shown in Figure 10. Here, the radar detectable distance was down to 592 m from 98,982 m using a direct flight (−99.4%). Leg distances with high probability of detection are shaded darker; other lengths are lighter.

The direct flight at a constant fixed altitude of 330 m resulted in the path shown in Figure 11, and a 60 m low-altitude direct flight resulted in the path shown in Figure 12.

As shown in Figure 12, the detectable distance drops to 25,198 m from 98,982 m as a result of flying at a terrain-following 60 m minimum low altitude. In the final run, shifting the weighting constant down to a value of

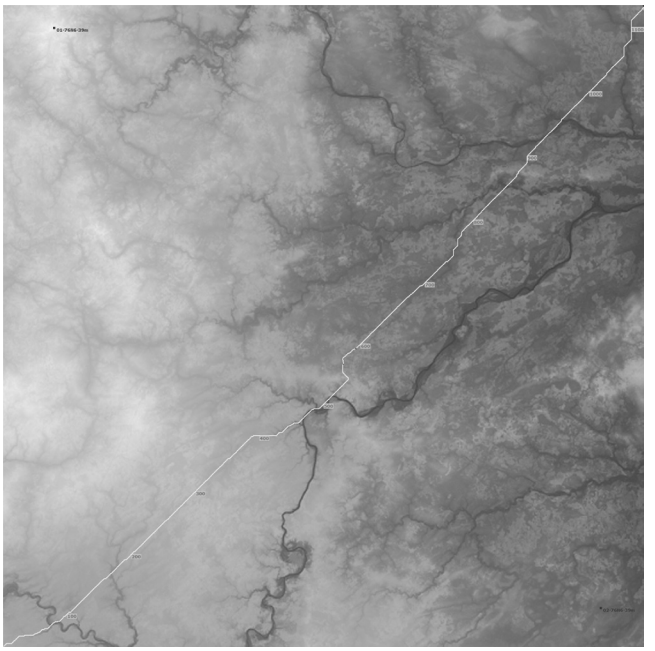

FIGURE 10 Flight path with two radars, $\alpha = 0.10$ total path distance = 150,233 m/detectable distance = 592 m.

$\alpha = 0.10$ then resulted in the path depicted in Figure 10 with only 592 m detectable.

A path on another map area shown in Figure 13 (centered on 57.49° N, 35.89° E) has a total length of 178,206 m, and a radar detectable equivalent distance of 10,065 m. Compared to a direct flight at a fixed altitude of 390 m, this shows a decrease of −87.6% in radar detectable distance and an increase of 26.1% in the total path distance. Compared to a terrain-following low-altitude (100 m) direct flight, it involves a drop of −78.7% in the detectable distance and an increase of 26.0% over that total distance. With a total radar detection time on the flight of over two minutes, however, this flight would still be well within the extreme danger estimate of a missile shoot-down risk benchmark.

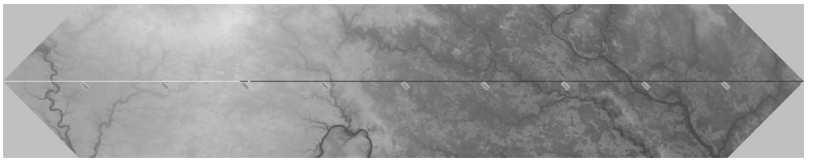

FIGURE 11 Direct fixed-altitude (330 m) flight with two radars. $\alpha = 1.00$, total path distance = 141,280 m, detectable distance = 98,982 m.

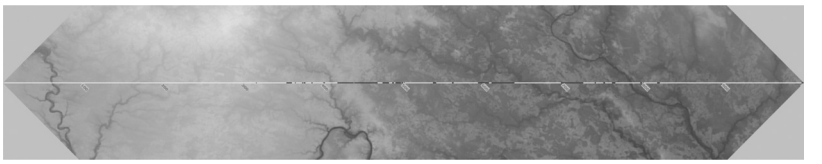

FIGURE 12 Direct terrain-following low-altitude (60 m minimum) flight with two radars. $\alpha = 1.00$, total path distance = 141,421 m, detectable distance = 25,198 m.

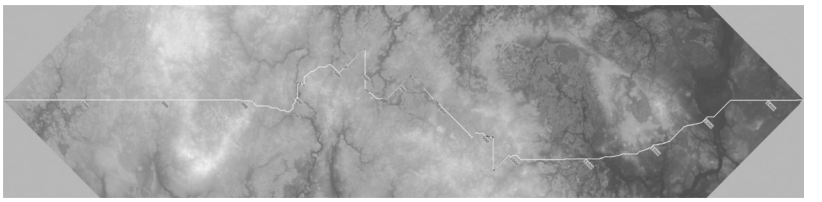

FIGURE 13 Flight path with two radars. $\alpha = 0.10$, total path distance = 178,206 m, detectable distance = 10,065 m.

CONCLUSION

A route-planning approach capable of various weighting values emphasizing different aspects of movement (reducing total path length, or relative safety from radar detection) was investigated. The described algorithm finds the least-cost path to a destination in terms of radar-detection probability and/or distance traveled while satisfying UAV maximum flight-range constraints. A possible result of this technique may be improved UAV routes that minimize detection probabilities over varied and complex terrain. In many situations, it was possible to decisively defeat radar tracking through the use of the developed route-planning technique.

REFERENCES

Andrew, M. 2009. *PLA mechanized infantry division air defense systems PLA point defense systems* (Technical Report). APA-TR-2009-0301, Air Power Australia, March 2009.

Barlow, G. J., C. K. Oh, and S. F. Smith. 2008. Evolving cooperative control on sparsely distributed tasks for UAV teams without global communication. In *Proceedings of the 10th annual conference on genetic and evolutionary computation*, ed. M. Keijzer, 177–184. New York: ACM.

De la Cruz, J. M., E. Besada-Portas, L. Torre-Cubillo, B. Andres-Toro, and J. A. Lopez-Orozco. 2008. Evolutionary path planner for UAVs in realistic environments. In *Proceedings of the 10th annual conference on genetic and evolutionary computation*, ed. M. Keijzer, 1477–1484. New York: ACM.

Flint, M., E. Fernandez, and W. D. Kelton. In press. Simulation analysis for UAV search algorithm design using approximate dynamic programming. *Military Operations Research.*

Hasircioglu, I., H. R. Topcuoglu, and M. Ermis. 2008. 3-D path planning for the navigation of unmanned aerial vehicles by using evolutionary algorithms. In *Proceedings of the 10th annual conference on genetic and evolutionary computation*, ed. M. Keijzer, 1499–1506. New York: ACM.

Kabamba, P., S. Meerkov, and F. Zeitz. 2006. Optimal path planning for unmanned combat aerial vehicles to defeat radar tracking. *Journal of Guidance, Control, and Dynamics* 29 (2): 279–288.

Kamrani, F., and R. Ayani. 2007. Using on-line simulation for adaptive path planning of UAVs. In *Proceedings of the 11th IEEE international symposium on distributed simulation and real-time applications*. 167–174. Washington, DC: IEEE Computer Society.

Karim, S., and C. Heinze. 2005. Experiences with the design and implementation of an agent-based autonomous UAV controller. In *Proceedings of the 4th international joint conference on autonomous agents and multiagent systems*, 19–26. Utrecht, the Netherlands: ACM.

Kopp, C., and C. S. Wallace. 2004. *TROPPO – A tropospheric propagation simulator* (Technical Report). School of Computer Science and Software Engineering, Monash University, Clayton, Australia, TR-2004/161, November 2004.

Kopp, C. 2004. *76N6 Clam shell low altitude acquisition radar; 5N66/5N66M/76N6/76N6E/40V6M/MD clam shell* (Technical Report). APA-TR-2004-1001, Air Power Australia.

Kopp, C. 2008. High energy laser air defence weapons. *Defence Today* December:40–42.

Kopp, C. 2009a. Helicopter combat survivability. *Defence Today* 7 (5): 39–41.

Kopp, C. 2009b. NKMZ 40V6M/40V6MD Universal Mobile Mast; Нкмз 40в6м/40в6мд Универсальная Передвижная Вышка (Technical Report), APA-TR-2009-0504, Air Power Australia.

Kopp, C. 2009c. KBTochmash 9K35 Strela 10 Self Propelled Air Defence System/SA-13 Gopher; Самоходный Зенитный Ракетный Комплекс КБточмаш 9К35 Стрела-10 (Technical Report), APA-TR-2009-0801, Air Power Australia, August, 2009.

Kopp, C. 2010. "Spatial Distribution of Fading Behaviour in Microwave Airborne Communications Links" (Draft journal paper including literature survey of refraction modeling).

Nikolos, Y., N. Tsourveloudis, and K. P. Valavanis. 2001. Evolutionary algorithm based 3-D path planner for UAV navigation. In *Proceedings of the 9th IEEE Mediterranean conference on control and automation*. Washington, DC: IEEE Computer Society.

Pajares, G., J. J. Ruz, P. Lanillos, M. Guijarro, J. M. de la Cruz, and M. Santos. 2008. Generación de Trayectorias y Toma de Decisiones para UAVs. *Revista Iberoamericana de Automática e Informática Industrial* 51:83–92.

Quigley, M., B. Barber, S. Griffiths, and M. A. Goodrich. 2005. Towards real-world searching with fixed-wing mini-UAVs. In *Proceedings of the 2005 IEEE/RSJ international conference on intelligent robots and systems*, 3028–3033. Washington, DC: IEEE Computer Society.

Russell, M. A., and G. B. Lamont. 2005. A genetic algorithm for unmanned aerial vehicle routing. In *Proceedings of the 2005 conference on genetic and evolutionary computation*, ed. H. Beyer, 1523–1530. New York: ACM.

Ruz, J. J., O. Arévalo, J. M. de la Cruz, and G. Pajares. 2006. Using MILP for UAVs trajectory optimization under radar detection risk. In *Proceedings of the 11th IEEE international conference on emerging technologies and factory automation,* 957–960. Washington, DC: IEEE Computer Society.

Ruz, J. J., O. Arévalo, G. Pajares, and J. M. de la Cruz. 2007. Decision making among alternative routes for UAVs in dynamic environments. In *Proceedings of the 12th IEEE international conference on emerging technologies and factory automation,* 997–1004. Washington, DC: IEEE Computer Society.

Ryan, J. L., T. G. Bailey, J. T. Moore, and W. B. Carlton. 1998. Reactive tabu search in unmanned aerial reconnaissance simulations. In *Proceedings of the 30th conference on winter simulation*, ed. D. J. Medeiros, E. F. Watson, J. S. Carson, and M. S. Manivannan, 873–880. Washington, DC: IEEE Computer Society.

Schelleng, J. C., C. R. Burrows, and E. B. Ferrell. 1933. Ultra-Short-Wave Propagation. *Proceedings of the institute of radio engineers* 21(3):427–463.

Schouwenaars, T., M. Valenti, E. Feron, and J. P. How. 2005. Implementation and flight test results of MILP-based UAV guidance, In *Proceedings of the IEEE aerospace conference*, 1–13. New York: IEEE.

USAF 1969. Flight Manual F-105D,F,G, T.O. 1F-105D-1, 30 June, 1969, revised 9 September, 1970.

USAF 1973. Flight Manual F-111E, T.O. 1F-111E-1, 30 June 1973.

Vincent, P., and I. Rubin. 2004. A framework and analysis for cooperative search using UAV swarms. In *Proceedings of the 2004 ACM symposium on applied computing*, 79–86. New York: ACM.

Zabarankin, M., S. Uryasev, and R. Murphey. 2006. Aircraft routing under the risk of detection. *Naval Research Logistics* l (538): 728–747.